

Dependence of Copper Concentration on the Properties of Cu₂ZnSnS₄ Thin Films Prepared by Electrochemical Method

E.M. Mkawi^{1,*}, K. Ibrahim¹, M. K. M. Ali¹ and Abdussalam Salhin Mohamed²

¹Nano-Optoelectronics Research and Technology Laboratory, School of Physics Universiti Sains Malaysia, 11800 Penang, Malaysia

²School of Chemical Sciences, Universiti Sains Malaysia, 11800 Penang, Malaysia

*E-mail: MOIZMERGHANIM@yahoo.com

Received: 3 October 2012 / Accepted: 29 November 2012 / Published: 1 January 2013

Quaternary Cu₂ZnSnS₄ (CZTS) thin films were fabricated as solar cell absorber layers via sequential electrodeposition method using a flexible copper plate as substrate. The CZTS thin films were grown with different copper salt concentrations and sulfurized in elemental sulfur vapor. The morphological, structural, compositional, and electrical properties of the films were investigated using X-ray diffraction, scanning electron microscopy, and energy dispersive X-ray spectroscopy, as well as by Raman scattering and Hall effect measurements. The results showed that the CZTS properties depend on the copper concentration in the precursor. The XRD patterns of the precursor showed the preferred orientation of the (112), (220), and (312) phases. The thin film showed a p-type conductivity, with a carrier concentration between $9.56 \times 10^{16} \text{ cm}^{-2}$ and $3.66 \times 10^{17} \text{ cm}^{-2}$, depending on the composition of the precursor mixture.

Keywords: Cu₂ZnSnS₄; Thin film; copper concentration; Electrochemical

1. INTRODUCTION

The quaternary compounds, CdTe and CuIn_{1-x}Ga_xSe₂ (CIGS), with 16.7% and 20.0% efficiencies, respectively, are the current commercialized materials for thin-film photovoltaic devices [1]. The production of such devices is difficult due to selenium toxicity and the lack of indium availability. Thus, researchers have turned their attention to alternative absorber compounds with similar properties [2]. A new p-type material, kesterite [Cu₂ZnSn(S/Se)₄], is a promising alternative for the fabrication of thin film solar cells. Cu₂ZnSnS₄ (CZTS) quaternary p-type semiconductors have recently attracted increasing attention from the scientific community. CZTS is derived from CIGS by replacing In with Zn, Ga with Sn, and Se with S. CZTS is a low-cost material formed from non-toxic

and abundant materials. CZTS has a direct band gap energy of approximately 1.5 eV, high absorption coefficient of $>104 \text{ cm}^{-1}$, and is environmentally friendly.

Several methods have been used to grow this p-type absorber layer, including thermal and electron-beam evaporation [3–5], co-evaporation [6–8], pulsed laser deposition [9–12], DC and RF magnetron sputtering [13–16], hybrid sputtering [17], screen printing [18], chemical vapor deposition [19], spray pyrolysis [20], sol-gel spin-coated deposition [21], and electrodeposition (co-electroplating) [22–24]. The electrodeposition method has gained particular interest because it is inexpensive, uses an environment-friendly process, produces large deposition areas, and grows films at room temperature. CZTS thin films are prepared by annealing Cu–Zn–Sn alloy precursor films with an S source (such as H_2S) in a N_2 atmosphere. Two different electrochemical methods are used to form CZTS thin films: (i) sequential electroplating (layer by layer deposition) and (ii) single-step electrodeposition method, wherein all electrolytes are mixed [25]. In the current study, CZTS p-type thin films were fabricated on a copper substrate using different salt copper concentrations via the sequential electrodeposition technique. The effect of the changes in copper concentration on the composition ratios of $\text{Cu}/(\text{Zn}+\text{Sn})$ and Zn/Sn in the precursor and on the final composition and properties of the CZTS thin film, such as its structural, morphological, compositional, and electrical properties, were investigated.

2. EXPERIMENTAL

A copper plate substrate (purity, 4N; thickness, 0.75 mm) and an exposure area of $2 \text{ cm} \times 2 \text{ cm}$ were used as the working electrode. A platinum electrode was used as counter electrode and an Ag/AgCl electrode was used as reference electrode. The copper oxide was removed through the Na_2O -CaO system from the copper plate [26]. CZTS thin films were deposited at room temperature for 20 min using an E-corder 401 potentiostat (Australia). The solutions were prepared using MilliQ water and metal salts (4 N). The deposited films were produced in an orderly fashion, Sn–Cu–Zn, at room temperature without stirring. The electrochemical deposition potential of the CZTS thin films was estimated using cyclic Voltammetry in an aqueous electrolytic bath. The Sn layer contained 1 M Sn (II) methanesulfonate (Aldrich) and $\leq 0.025 \text{ vol\%}$ Empigen BB, obtained from Aldrich and Sigma (Germany), respectively. The zinc electrolyte contained 2 M KCl ($\geq 99.0\%$, Sigma) and 50 mM ZnCl_2 (98%, Aldrich).

Copper electrolyte containing different concentrations of copper salt (0.01 M, 0.02 M, 0.03 M, 0.04 M of $\text{Cu}(\text{NO}_3)_2$ ($\geq 98\%$), 0.2 M Sorbitol ($\geq 99.5\%$), and $\leq 0.025 \text{ vol\%}$ Empigen BB was purchased from Sigma (Germany).

The samples were rinsed with deionized water and dried under flowing N_2 after the deposition of the layers. The precursors were loaded into a graphite container inserted into a quartz tube furnace. The precursors were initially annealed at $100 \text{ }^\circ\text{C}$ for 10 min to dry and to ensure that the reaction between the precursor surfaces and S occurs completely. The temperature was increased to $580 \text{ }^\circ\text{C}$ for 2 h in a flowing N_2 atmosphere, at a ramping rate of $100 \text{ }^\circ\text{C}/\text{min}$ with 50 mg of S. Afterward, the precursors were allowed to cool naturally.

The total thickness of the precursor after annealing was approximately 1.5 μm . The crystallographic phase of the thin films was observed using X-ray diffraction (XRD, PANalytical X'pert PRO MRD PW3040-Netherlands). The cross-sectional and surface morphology, as well as the composition of the films, were determined by scanning electron microscopy (SEM) and energy dispersive X-ray spectroscopy [EDX, JSM-6460 LV(Japan)]. Carrier concentration and Hall mobility were determined using a Hall-effect measurement system [Accent/HL 5500 PC (UK)]. Raman spectroscopy was used to complement the study of the different crystallographic phases in the samples [Yvon HR800 UV (France)].

3. RESULTS AND DISCUSSION

The copper plate used to fabricate CZTS in this study has the following advantages. The copper plate is used simultaneously as a substrate and a back contact, thus, it entails low cost. The adherence between the copper substrate and the CZTS thin film is also high. Moreover, the copper substrate is flexible, with a resistivity of 25 $\mu\Omega\text{cm}$, which yields a small potential variation along the length of the substrate.

The different morphological characteristics and thicknesses of the samples are attributed to the variations in the deposition conditions, such as how fast the electrons are transferred from the electrode to the depositing ion [27]. Regulating the flux of ions to the substrate by maintaining a constant distance between the platinum electrode and the substrate at 1.5 cm for all layers is necessary to control the uniformity of the depositions on the copper substrate. A rotating disc electrode was used to improve the large-scale uniformity of the CZTS film, with 150 rotations per min for all layers.

3.1. Composition analysis

Table I shows the chemical compositions of the film grown at 580 $^{\circ}\text{C}$ for 2 h, where the values of the Cu/(Zn+Sn) and the Zn/Sn ratios in the synthesized CZTS thin film are also presented. The Cu/(Zn+Sn) ratios in the precursor mixture were changed from 0.98 to 1.22, and the Zn/Sn composition ratios were changed from 1.02 to 1.08. The Cu/(Zn+Sn) ratio in the precursor film increased with the increase in Cu concentration in the solution, thereby increasing the Cu-rich film.

Table I. Elemental composition of CZTS films with Copper concentration

Copper concentration In solution (M)	(Cu/Zn+Sn)	Ratio	
		Zn/Sn	S/metal
(a) 0.01	0.98	1.08	0.94
(b) 0.02	0.98	1.06	0.90
(c) 0.03	1.01	1.02	0.91
(d) 0.04	1.02	1.07	0.96

After annealing, the Cu/ (Zn+Sn) ratio in CZTS thin films was > 1 , close to the ratio required for stoichiometric CZTS formation, indicating that the films are Cu-rich and Zn-poor. The EDX analysis of the sulfurized exhibited a S-poor composition [S poor (S/Metal < 1)], indicating that S was sufficiently incorporated with the other metals into the precursors. The heat treatment replaced much of the oxygen with S [28]. In addition, the S/metal ratio remained almost constant in all CZTS films due to the evaporation of tin sulfide. The Cu/(Zn+Sn) and the Zn/Sn ratios in the films slightly increased after sulfurization. The chemical composition of the CZTS thin film greatly influenced its properties. The surface morphology of the annealed CZTS thin film was investigated using SEM.

3.2. Morphological characterization

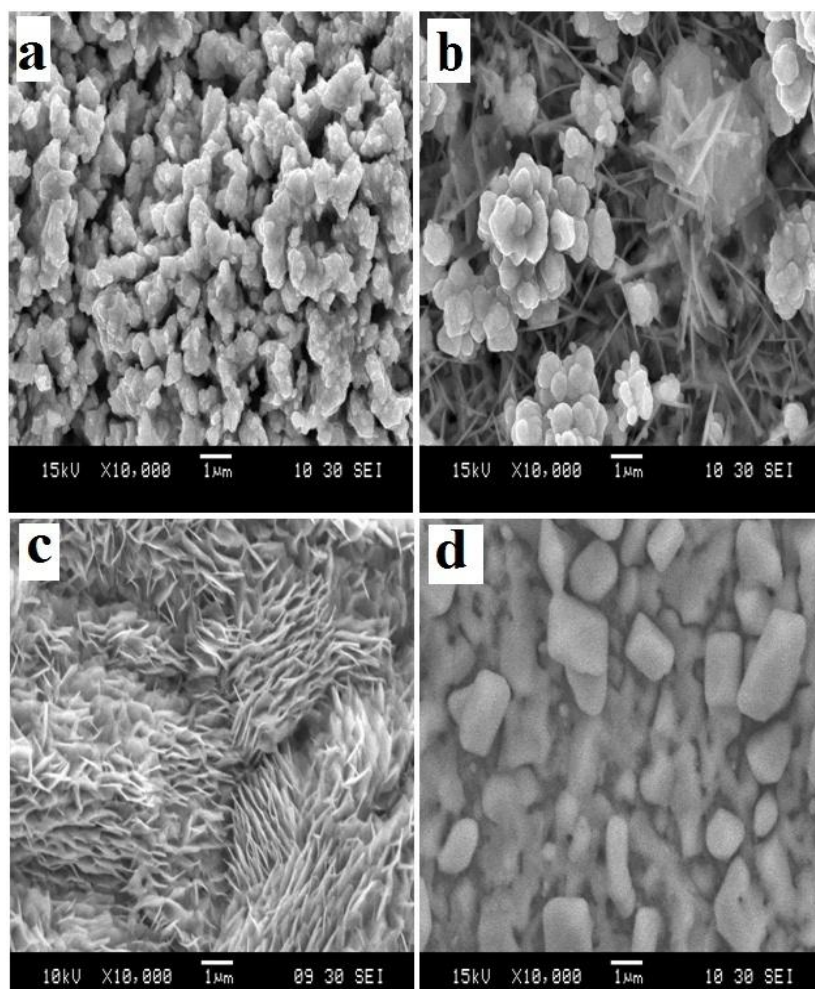


Figure 1. SEM images of electrochemical deposition of CZTS film layers (a) copper nanoparticles on the thin layer (b) zinc micro flower on the copper layer (c) tin nanowire on copper plate substrate (d) CZTS microparticles

Fig. 1 shows the SEM images of the CZTS films deposited via the electrochemical method on the copper plate substrate grown at 580 °C with a Sn/Cu/Zn precursor. Fig. 1(a) shows the occurrence of copper nanoparticle agglomeration as a result of the electrochemical deposition of the copper

electrolytes onto the Sn layer. The surface was non-uniform with a homogeneous size distribution and voids, cavities were observed. Fig. 1 (b) shows the formation of zinc micro flowers when the zinc layer was deposited after 1 min at room temperature. Fig. 1(c) illustrates the formation of Sn nanowires after 1 min of deposition on the copper plate substrate. Fig. 1 (d) shows the formation of CZTS microparticles after annealing for 2 h.

The SEM results of the as-synthesized samples show that the quaternary chalcogenides particles were largely aggregated. These particles are composed of primary crystallites with sizes larger than 1 μm . The large crystallite size may be attributed to the chemical homogeneity of the various components into the precursors and the copper substrate.

The precursor was uniform, and the size of the compact grains ranged from 800 nm and 1 μm , with an average diameter of approximately 500 nm. The conversion efficiency of the solar cells increased with an increase in the grain size of the absorber layer material. Therefore, larger grains are required for the fabrication of highly efficient solar cells. Voids on the absorber layer in the thin film solar cells lead to low conversion efficiency because the generated carriers are disturbed at both grids [29]. The large grain size in the absorber layer is important to both the minority carrier diffusion length and the recombination potential in polycrystalline thin film solar cells.

3.3. Structural characterization

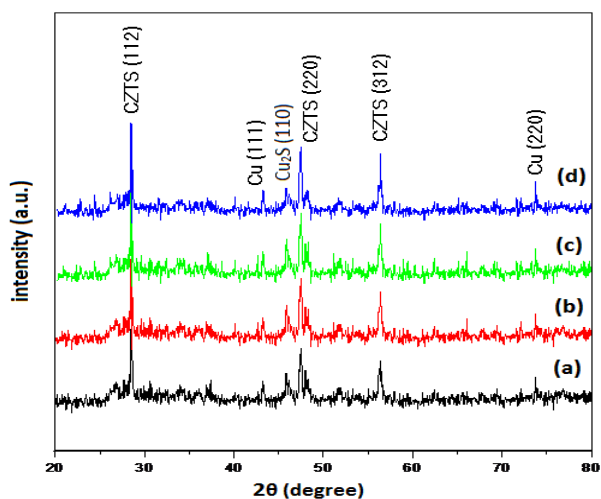


Figure 2. X-ray diffraction patterns of CZTS thin films with copper concentrations (a) 0.01 (b) 0.02 (c) 0.03 (d) 0.04 M. The XRD patterns of the CZTS film heated and sulfurized at 580 °C for 2 h are shown in Fig. 2. The diffraction angle 2θ varied from 20° to 80°. Fig. 2 also shows the XRD patterns of the as-deposited precursor and the samples obtained at various copper concentrations. The XRD pattern for the sample shown in Fig. 2 (a) indicates that the film is composed of CZTS and some secondary phases. The thin film contains kesterite structures, with peaks attributable to the (112), (220), and (312) phases, corresponding to the kesterite structure of the CZTS. These planes were observed clearly in all samples, indicating the formation of kesterite CZTS phase. A preferred (112) orientation was observed in all deposited films, which agrees with the reported features of CZTS [30–31]. The copper peaks appeared at (111) and (220) ($2\theta = 73.88$).

Peaks in the secondary phase of Cu_2S occurred at (110) and (103), which were observed in the XRD results when the films were prepared with higher $\text{Cu}/(\text{Zn}+\text{Sn})$ ratios. The growth of Cu_{2-x}S on the Cu-rich side of the compositions is in agreement with the phase diagram obtained by Oleksyuk et al. [32]. The growth of Cu_2S may assist in CZTS film formation through liquid assisted grain growth, resulting in large grains and compact CZTS films [33].

The copper sulfide phase can be removed from the CZTS surface by immersing the samples in a KCN solution [34]. The XRD patterns of the copper concentration in Figs. 2 (b), 2 (c), and 2 (d) show the same result for the concentrations in Fig. 2 (a), with an increase in sharpness from Fig. 3 (b) to Fig. 3 (d). The concentration of the CZTS peaks were sharp and well defined, as shown in Fig. 2 (d). The CZTS phase became the dominant phase and the Cu_2S peak was reduced. This decrease of the Cu_2S peak, shown in Fig. 3 (d), suggests that the Cu_2S phase was fully consumed in the formation of the CZTS film, indicating that the thin film was well-grown, with good crystallinity. XRD analysis was used to calculate the lattice parameters for the sample in Fig. 3 (d), where $a=5.427 \text{ \AA}$ and $c=10.848 \text{ \AA}$. The size of the crystalline particles at different copper concentrations was given by the Scherrer formula:

$$D = \frac{0.9 \lambda}{\beta \cos \theta}$$

Where D is the diameter of the crystalline particles, θ is the Bragg angle, β is the width of the dominant peak in radians at half its intensity, λ is the wavelength of the X-ray used [35].

The results showed a significant increase in the grain size when the films were grown in high copper concentration because the increase in copper concentration changed the compositional ratios of $\text{Cu}/(\text{Zn}+\text{Sn})$ [Table (2)].

Table 2. Change crystallite size of variation in copper concentration

Sample concentration (M)	crystallite size film (nm)
(a) 0.01	47
(b) 0.02	51
(c) 0.03	59
(d) 0.04	62

XRD does not allow the distinction between the CZTS and ZnS, thus, the Cu_2SnS_3 structures, i.e., the XRD peaks from (112), (200), (204), and (312) planes of the CZTS, coincide with the XRD peaks from (111), (200), (220), and (311) planes of ZnS, respectively [36].

Raman investigation was performed to fully characterize the samples, Raman characterization is crucial to complete the identification of the CZTS structure.

Fig. 3 shows the Raman spectra of the samples obtained at various copper concentrations, in which all samples showed the major peaks corresponding to the CZTS, with a strong peak positioned at 339 cm^{-1} , which is in agreement with the results of previous studies [37]. Figs. 3 (a) and 3 (b) show that both spectra exhibited a major peak at 339 cm^{-1} , corresponding to the CZTS phase, and a broad

peak at 304 cm^{-1} and 361 cm^{-1} , corresponding to Sn_2S_3 and CZTS, respectively [38 ,39]. The $\text{Cu}_2\text{ZnSnS}_4$ phase resulted from the binary phases of Cu_2S – SnS_2 – ZnS or from a solid state reaction of the ternary Cu_2SnSn_3 and ZnS [40].

Schurr et al. Showed that the presence of SnS_x induced the crystallization of CZTS. They indicated that the presence of this melt during CZTS crystallization enhanced the grain size of the films [41]. Fig. 3 (c) shows a sharp peak at 361 cm^{-1} (CZTS) , with a weak peak at 238 cm^{-1} and 368 cm^{-1} attributed to CZTS.

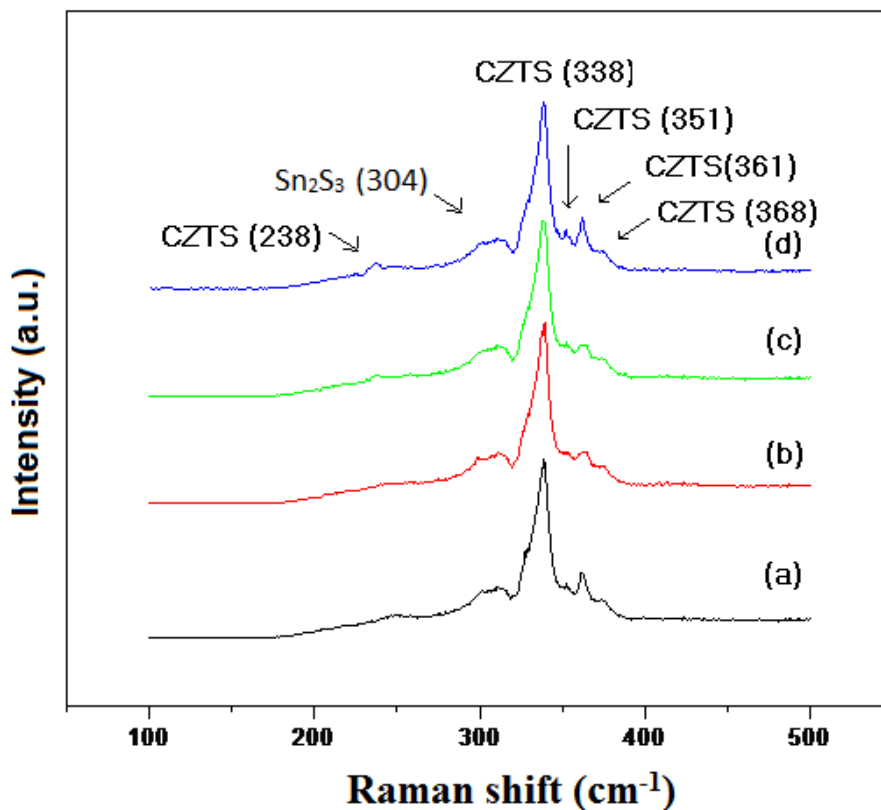


Figure 3. Raman scattering results for the samples with different copper concentration (a) 0.01 (b) 0.02 (c) 0.03 (d) 0.04 M

Fig. 3 (d) The Raman spectra clearly show the peak positions at 238 cm^{-1} , 338 cm^{-1} , 351 cm^{-1} , 361 cm^{-1} , and 368 cm^{-1} respectively, corresponding to the CZTS phase. The presence of these five peaks in the Raman spectra indicates the formation of the CZTS phase. In addition, the sharp and strong major peak indicates the good crystalline quality of the compound.

Peaks at 271 cm^{-1} and 352 cm^{-1} attributable to ZnS in the Raman spectrum were not observed, indicating the absence of the ZnS phase in the sample and the formation of good quality single phase CZTS.

3.4. Electrical characterization

Table 3 shows the electrical properties of the CZTS film after heating and sulfurization at 580 °C for 2 h on the copper plate substrate with different copper concentrations. The thin films exhibited a p-type conductivity. The measured resistance decreased from 9.82×10^3 to $9.67 \times 10^2 \Omega / \text{sq}$ with increasing Cu content in the precursor, indicating that main Cu-rich and Sn-rich powders have the lowest grain resistance [42].

Table 3. Electrical properties of the CZTS films of varying in copper concentration

Samples with different Cu concentration (M)	Sheet resistant R_s (Ω / sq)	Resistivity ρ ($\Omega\text{-cm}$)	Carrier concentration N (cm^{-3})	Hall mobility μ_H ($\text{cm}^2/\text{v.s}$)
(a) 0.01	9.82×10^3	12.5	9.56×10^{16}	66.5
(b) 0.02	6.56×10^3	8.57	1.06×10^{17}	52.3
(c) 0.03	2.78×10^3	7.33	2.43×10^{17}	44.9
(d) 0.04	9.67×10^2	6.98	3.66×10^{17}	39.8

The carrier concentration increased from 9.56×10^{16} to $3.66 \times 10^{17} \text{ N (cm}^{-3}\text{)}$ with the increase in Cu content in the precursor. The electrical properties of the films were attributed to the enhanced grain size. The large grains in the material reduced the grain boundaries, thus effectively reducing the recombination of the charge carriers. The crystallite size increased with the increase in copper concentrations [43], similar to that in previous studies [44,45]. The electrical properties of the electrochemical deposition of the CZTS layer agree with the requirements for potential application in thin film solar cell fabrication. In addition, the electrochemical deposition technique proposed in this study can be used to fabricate CZTS layers on flexible substrates.

4. CONCLUSIONS

CZTS thin films were successfully deposited on a copper plate substrate using the electrochemical technique. The processes were completed by the sulfurization of stacked metallic layers in an atmosphere of N_2 with S Vapor. The copper plate can be used as a substrate and a back contact at the same time. Good atomic stoichiometry of the compound was obtained in the sample prepared with different copper concentrations. The elemental composition was close to the stoichiometry of the CZTS thin film. The chemical homogeneity of the precursors and the copper substrate was greatly affected by the quality of the crystal growth and crystallite size of the particles. The results confirmed that CZTS was present in the thin film, with kesterite structure. The thin film showed peaks attributed to the (112), (220), and (312) phases, as well as small traces of copper sulfide.

The resulting CZTS film exhibited p-type conductivity and suitable electrical properties for the fabrication of thin film solar cells.

ACKNOWLEDGEMENTS

This work was supported by the Nano-optoelectronics Research Laboratory, School of Physics: Universiti Sains Malaysia under grant number 203/PSF-6721001, We would like to express our great thanks for all who concerned with this work.

References

1. S. C. Riha, B.A. Parkinson, A. L. Prieto, *J. American Chemical Society*, 131 (2009) 12054–12055.
2. P. A. Fernandes, P. M. P. Salome, A. F. Cunha, *Semicond. Sci. Technol*, 24 (2009) 105013.
3. Y.L. Zhou, W.H.Zhou, Y.F. Du, M. Li, S.X. Wu, *Materials Letters*, 65 (2011) 1535–1537.
4. J. Madarasz, P. Bombicz, M. Okuya, S. Kaneko, *Solid State Ionics*, 142 (2001) 439–446.
5. K. Wang, O. Gunawan, T. Todorov, B. Shin, S. J. Chey, N. A. Bojarczuk, D. Mitzi, S. Guha, *Applied Physics Letters*, 97 (2010)143508.
6. T. Tanaka, A. Yoshida, D. Saiki, K. Saito, Q. Guo, I. Nishio, T. Yamaguchi, *Thin Solid Films*, 518 (2010) S29–S33.
7. B. Schubert, B. Marsen, S. Cinque, T. Unold, R. Klenk, S.Schorr, H.Schock, *Photovolt: Res. Apple*, 19 (2011) 93–96.
8. T. Tanaka, D.Kawasaki, M.Nishio,Q. Guo, H. Ogawa, *Phys. Stat. sol. (c)*, 8 (2006) 2844–2847.
9. K. Sekiguchi, K. Tanaka, K. Moriya, H. Uchiki, *phys. Stat. sol. (c)*, 3 (2006) 2618–2621.
10. R. A. Wibowo, E. S. Lee, B. Munir, K. H. Kim, *Phys. Stat. sol. (a)*, 204 (2007) 3373–3379.
11. I.Ohkubo, H.M. Christen, P. Khalifah, S. Sathyamurthy, H.Y. Zhai,C.M. Rouleau, D.G. Mandrus, D.H. Lowndes, *Applied Surface Science*, 223 (2004) 35–38.
12. A.V. Moholkar, S.S. Shinde, A.R. Babar, K. Simb, H.Leeb, K.Y. Rajpure, P.S. Patil, C.H. Bhosale, J.H. Kim, *Alloys Compounds*, 509 (2011)1-17.
13. H. Nukala, J. L. Johnson, A. Bhatia, E. A. Lund, W. M. Hlaing, M. M. Nowell, L. W. Rieth, M. A. Scarpulla, *Mater. Res. Soc. Symp. Proc*, 1268 (2010) 03-04.
14. P.A. Fernandes, P.M.P. Salomé, A.F. da Cunha, B.Schubert, *Thin Solid Films*, 519 (2011) 7382.
15. F. Liu, YiLi, K.Zhang, B.Wang, C.Yan, Y. Lai, Z. Zhang, J. Li, Y. Liu, *Solar Energy Materials & Solar Cells*, 94 (2010) 2431–2434.
16. J. Seola, S. Lee, J. Lee, H. Namb, K.Kim, *Solar Energy Materials & Solar Cells* 75 (2003) 155–162.
17. T. Tanaka, T. Nagatomo, D. Kawasaki, M. Nishio, Q. Guo, A.Wakahara, A.Yoshida, H.Ogawa, *Phys. Chem. Solids* 66 (2005) 1978–1981.
18. Z. Zhoun, Y. Wang, D. Xu, Yafei Zhang, *Solar Energy Materials & Solar Cells* 94 (2010) 2042–2045.
19. K. Ramasamy, M. A. Malik and Paul O'Brien, *chem.commun* 48 (2011) 1170-1172.
20. Y. B. K. Kumar, G. S. Babu, P.U. Bhaskar, V. S. Raja, *Phys. Status Solidi (A)* 206 (2009) 1525–1530.
21. M. Y. Yeh, C. C. Lee, D. S. Wu, *J Sol-Gel Sci Techno*, 52 (2009) 65–68.
22. C.P.Chan, H. Lam, K.Y. Wong, C. Surya, *Mater. Res. Soc. Symp. Proc*, 1123 (2009) 05-06.
23. S.C.Riha,S.J.Fredrick, J.B.Sambur, Y. Liu, A. L. Prieto, B. A. Parkinson, *ACS Appl. Mater. Interfaces*, 3 (2011) 58–66.
24. J.J. Scragg, D. M. Berg, P. J. Dale, *Journal of Electro analytical Chemistry*, 646 (2010) 52–59.
25. S.M. Pawara, B.S. Pawar, A.V. Moholkar, D.S. Choi, J.H. Yun, J.H. Moon,S.S. Kolekar, J.H. Kim, *Electrochimica Acta*, 55 (2010) 4057–4061.

26. P. Coursol, B. Davis, A. Roy, M. Lebel, *Jom*, 57 (2005) 64-67.
27. M. Kurihara, D. Berg, J. Fischer, S. Siebentritt, P. J. Dale, *Phys. Status Solidi C* , 6 (2009) 1241–1244.
28. A. Wangperawong , J.S. King, S.M. Herron, B.P. Tran, K. Pangan-Okimoto, S.F. Bent, *Thin Solid Films* ,519 (2011) 2488–2492.
29. S. W. Shin, S.M. Pawar, C. Y. Park , J. H. Yun , J. H. Moon, J. H. Kim , J. Y. Lee, *Solar Energy Materials & Solar Cells* .95 (2010)3202-3206.
30. Y.liu,M.Ge,Y.Yue,Y.Sun,Y.Wu,X.Chen,N.dai, *Phys.Status Solidi* 3(2011) 113-115.
31. H. Araki, Y. Kubo, K. Jimbo, W. S. Maw, H. Katagiri, M. Yamazaki, K. Oishi, A. Takeuch , *Phys. Status Solidi* 5 (2009) 1266-1268 .
32. I. Olekseyuk, I. Dudchak , L. Piskach, *Journal of Alloys and Compounds*, 368 (2004) 135-143.
33. R.B.V. Chalapathy, G. S. Jung, B.T. Ahn, *Solar Energy Materials & Solar Cells* , 95 (2011) 3216–3221
34. K. Muska, M. Kauk, M. Altosaar, M. Pilvet, M. Grossberg, O. Volobujeva , *Energy Procedia* 10 (2011) 203 – 207.
35. T. Kucukomeroglu, E. Bacaksiz, C. Terzioglu, A. Varicli, *Thin Solid Films*. 516 (2008) 2913–2916.
36. H. Katagiri, K. Jimbo, W.S. Maw, K. Oishi, M. Yamazaki, H. Araki, A. Takeuchi, *Thin Solid Films* , 517 (2009) 2455–2460.
37. S.M.Pawar, A.V.Moholkar, I.K.Kim, S.W.Shin, J.HooJ.I.Rhee,J.H.Kim, *Curr.Appl Phys*,10 (2010) 565–569.
38. K .Wang, B. Shin, K. B. Reuter, T. Todorov, D. B. Mitzi, S. Guha , *Applied Physics Letters*, 98 (2011) 051912 - 051912-3 .
39. M .Himmrich, H.Haeusler, *Spectrochim Acta* 9(7)(1991) 33–42.
40. F. Herbert, R. Hock, *Thin Solid Films*, 515 (2007)5953–5956.
41. R.Schurr,A.Holzing,S.Jost,R.Hock,T.Voss,J.Schulze,A.Kirbs,A.Ennaoui,M.Steiner,AWeber,I.K.chau,H.W.Schock , *Thin Solid Films* ,517(2009)2465–2468.
42. T. Tanaka, A. Yoshida, D.Saiki, K.Saito ,Q. Guo, M. Nishio , T. Yamaguchi, *Thin Solid Films* 518 (2010) S29-S33.
43. T. Prabhakar, N. Jampana, *Solar Energy Materials & Solar Cells* ,95 (2011) 1001–1004.
44. Z. Zhoun, Y. Wang, D. Xu, Y. Zhang, *Solar Energy Materials & Solar Cells* , 94 (2010) 2042–2045.
45. A. Weber, R. Mainz, H.W. Schock, *Appl. Phys.* 107 (2010) 013516-1-6.